Fe-Catalyzed Aziridination Is Governed by the Electron Affinity of the Active Imido-Iron Species

Guillaume Coin, Ranjan Patra, Sujoy Rana, Jyoti Prasad Biswas, Patrick Dubourdeaux, Martin Clémancey, Sam P. de Visser, Debabrata Maiti, Pascale Maldivi, Jean-Marc Latour

Fe-catalyzed aziridination is governed by the electron affinity of the active imido-iron species

Guillaume Coin,[a,b,$,&] Ranjan Patra,[a,c,d,&] Sujoy Rana,[e] Jyoti Prasad Biswas,[f] Patrick Dubourdeaux,[a] Martin Clémancey,[a] Sam P. de Visser,[g] Debabrata Maiti,[f] Pascale Maldivi,[c]* and Jean-Marc Latour[a]**

[a] Univ. Grenoble Alpes, CEA, CNRS, IRIG, LCBM, 38000 Grenoble, France,

E-mail: jean-marc.latour@cea.fr

[b] Univ. Grenoble Alpes, CEA, CNRS, DCM, 38000 Grenoble, France

[c] Univ. Grenoble Alpes, CEA, CNRS, IRIG, DIESE, SYMMES, 38000 Grenoble, France

E-mail: pascale.maldivi@cea.fr

[d] Amity Institute of Click Chemistry Research & Studies (AICCRS), Amity University, Sector-125, Noida, India

[e] Department of Chemistry, University of North Bengal, Raja Rammohunpur, Darjeeling, West Bengal-734013, India

[f] Department of Chemistry, IIT Bombay, Powai, Mumbai-400076, India

E-mail: dmaiti@chem.iitb.ac.in

[g] Manchester Institute of Biotechnology and Department of Chemical Engineering and Analytical Science, The University of Manchester, 131 Princess Street, Manchester M1 7DN, United Kingdom

$ Present address: Department of Chemistry and Applied Biosciences, ETH Zürich, 8093 Zürich, Switzerland

& These authors contributed equally

KEYWORDS: aziridination, iron complexes, catalysis, Mössbauer spectroscopy, DFT calculations, reaction profile, electron affinity

ABSTRACT. Aziridination has very recently been found to be catalyzed by heme and non-heme Fe enzymes opening the way to biotechnological developments. However, its mechanism is not fully understood owing to contrasting behaviors exhibited by several Fe catalysts. Indeed, whereas a few Fe catalysts exhibit an activity dominated by inductive effects, the activity of others reveal significant and even dominant radical delocalization. Therefore, no clear and general rationale of aziridination has yet emerged. Elaborating on our previous studies we anticipated that replacing two pyridines of a pentanitrogen ligand by two quinolines would enhance the electron affinity of the corresponding imido Fe^{IV} active species and hence its

aziridination activity. This proved to be the case and Hammett correlations indicate an electrophilic active species and dominant inductive effects. The calculated reaction profile points to a two-step mechanism with the formation of the first C-N bond being rate-determining and involving a strong charge transfer in the transition state. The aziridine ring closure in the second step is almost barrierless. A clear correlation of aziridination yields with calculated EA for Fe-catalysts indicate that the dependence of aziridination efficacy on EA of active species is a quite general feature. To generalize this analysis we re-investigated a catalyst exhibiting radical delocalization dominance. Indeed a similar two-step mechanism was found which involves a partial charge transfer in the C-N bond formation as all other cases. The interesting point is that owing to the strong steric hindrance of the catalyst substitution, the aziridine ring closure of the intermediate benzylic radical (second step) becomes rate-determining, thus explaining the dominance of radical delocalization effect. Eventually, a general aziridination two-step mechanism has been rationalized and EA thus appears as the key descriptor for Fe-based catalytic aziridination that can be used in a predictable way.

INTRODUCTION

The formation of carbon - nitrogen bonds is central to the synthesis of numerous biologically active molecules which are of utmost pharmaceutical and agricultural interest. In this respect nitrene transfer reactions offer a viable alternative to heteroatom coupling methods which require pre-functionalization of the substrate.[1] However, they require metal catalysts which most often involve expensive and toxic noble metals such as Rh,[2,3] Ru[4,5] and Pd.[6] Therefore their

replacement by more "eco-friendly" metals is continuously motivating a strong research effort. Numerous nitrene transfer catalytic systems based on first-row transition metals have thus been reported in the past decade, namely with Cu,[7,8] Co[9,10] and most notably Fe.[5,11] The latter is a particularly useful catalyst from an industrial and environmental perspective since Fe appears as the ultimate cheap, available and non-toxic metal.[12–14] However, iron-catalyzed nitrene transfer reactions are poorly understood, albeit it is commonly admitted that they involve a high-valent iron-imido species,[11] by analogy with oxygenase enzymes.[15] This view is supported by the observation that natural as well as engineered enzymes can catalyze nitrene transfers.[16–19] Numerous iron-imido and iron-imidyl complexes have been isolated over the past decade[20–30] but few studies of their catalytic activity have been reported. More recently, however, a few systems were considered more in depth and their nitrene transfer ability assessed in sulfimidation reaction[28,29,31] or $H^{\bullet}$ abstraction.[28,29,31–33]

In particular, Sastri, de Visser and their coworkers[31,34] used in depth experimental and computational studies to investigate the reactivity of the imido $[(N4Py)Fe^{IV}(NTs)]^{2+}$ species $\mathbf{1^{IV}{=}NTs^{2+}}$ (Ts = p-tosyl, Scheme 1) previously reported by Que Jr. and coll..[21] Comparison with its oxo counterpart $[(N4Py)Fe^{IV}(O)]^{2+}$ $\mathbf{1^{IV}{=}O^{2+}}$ revealed a higher activity of $\mathbf{1^{IV}{=}NTs^{2+}}$ in atom transfer to thioanisoles but a higher activity of $\mathbf{1^{IV}{=}O^{2+}}$ in $H^{\bullet}$ abstraction. Moreover it was shown that NTs transfer leading to sulfimidation occurred through a long range electron transfer. This was supported by the calculated values of the electron affinities (EA) of the active Fe species. Indeed, the value for the imido complex $\mathbf{1^{IV}{=}NTs^{2+}}$ is significantly higher than that of the oxo analog (EA_{1NTs} = 134.5 kcal mol^{-1} vs EA_{1O} = 117.6 kcal mol^{-1} for $\mathbf{1^{IV}{=}O^{2+}}$). Nam, Fukuzumi and coworkers[35] were able to measure the redox potential of the $[(N4Py)Fe^{III}(NTs)]^{+}$/ $[(N4Py)Fe^{IV}(NTs)]^{2+}$($\mathbf{1^{III}{=}NTs^{+}}$/$\mathbf{1^{IV}{=}NTs^{2+}}$) couple and the experimental value (1.04 Vsce) is in

excellent agreement with the calculated one (1.06 Vsce), which supports the validity of the computational study. In an independent study, Nam and coll. isolated complex **3**$^{-}$ [(TAML)Fe^{V}(NTs)]$^{-}$ (Scheme 1) and oxidized it to **3** [(TAML$^{\bullet}$)Fe^{V}(NTs)].[28,29] By comparing the reactivities of the two complexes in thioanisole sulfimidation and H$^{\bullet}$ abstraction, they showed that oxidation of the ligand increased the sulfimidation rate by four orders of magnitude whereas it increased H$^{\bullet}$ abstraction only 2.5 times. This difference in activity enhancement was assigned by

Scheme 1. Various high-valent non-heme Fe catalysts.

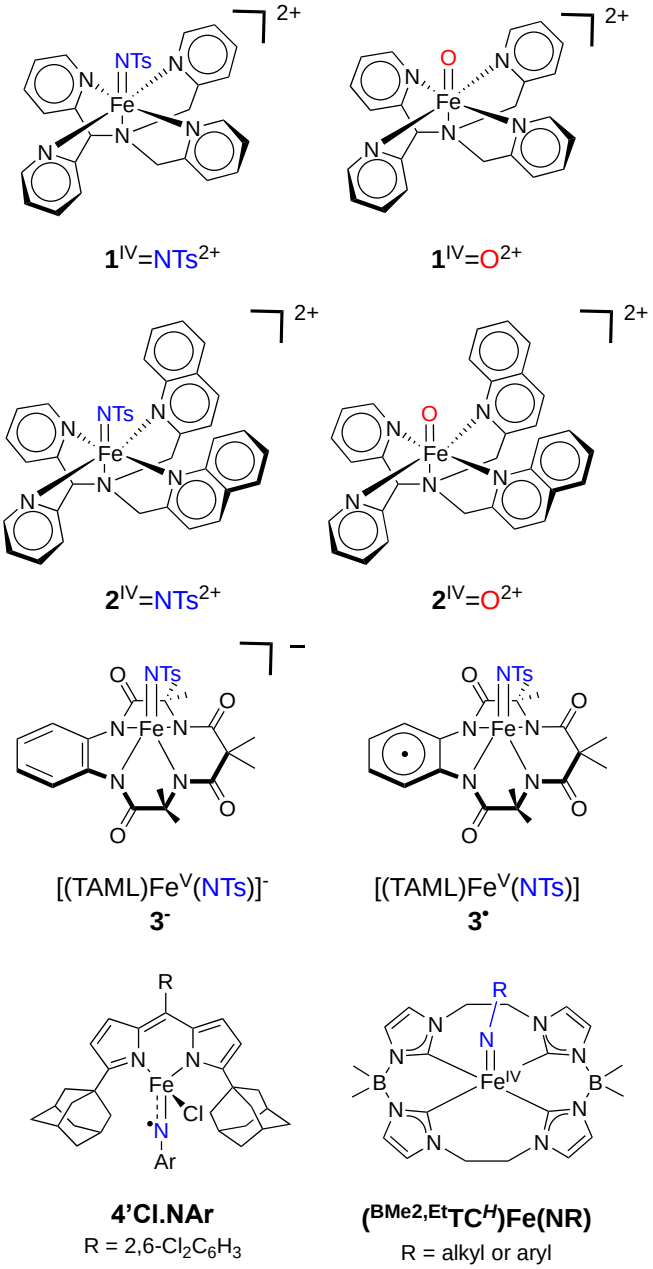

DFT calculations to the fact that oxidation of the ligand increased drastically the electron affinity of the complex (EA_3 = 122.8 kcal mol^{-1} vs EA_{3^-} = 103.9 kcal mol^{-1}) whereas it increased moderately the Bond Dissociation Energy (BDE) of the reduced species, which is a key factor for H$^{\bullet}$ abstraction (BDE_{3^-} = 81.9 kcal mol^{-1} vs BDE_{3} = 85.2 kcal mol^{-1}).[29] Conversely to the TAML case, Betley and coll. compared the activity of the dipyrromethene Fe imido complex ($^{Mes}L^{Ph4}$)Fe^{III}(NAd) **4^{III}=NAd** (Mes = 1,3,5-trimethylphenyl, Ph4 = 1,3,5-triphenylphenyl) with

its Fe imidyl counterpart ($^{Mes}L^{Ph4}$)Fe^{III}Cl(-$^{\bullet}$NAd) **4^{III}Cl-$^{\bullet}$NAd** (Scheme 1). They noted that one-electron oxidation of the imido ligand caused a rate enhancement of $H^{\bullet}$ abstraction by two orders of magnitude. Unfortunately neither EA nor BDE were calculated.

By contrast no comparable mechanistic information was available on iron-catalyzed aziridination, either for heme[36] or non-heme[37] based catalysts. This reaction bears a strong interest owing to the specific intrinsic biological activities of aziridines and their involvement as intermediates in multistep amine syntheses.[38] A few limited mechanistic studies of iron-based catalytic aziridination systems have been reported in the past decade but a rationalization of their activities is still lacking, owing to the widely different if not opposite behaviors reported.[39–46] Using a similar dipyrromethene ligand ($^{DCP}L^{Ad}$)Fe (DCP = 2,6-dichlorophenyl, Ar = p-tBu-Ph), Betley and coll. reported that the system ($^{DCP}L^{Ad}$)FeCl / AdN_3 catalyzes the aziridination of various olefins (used as reaction solvent) probably through the formation of ($^{DCP}L^{Ad}$)FeCl(NAd) **4'^{III}Cl-$^{\bullet}$NAd**. Hammett correlations supported a two-step mechanism dominated by radical delocalization effects and negligible inductive electronic influence.[41] This behavior strongly departs from that described for styrene aziridination by phenyltosyliodinane by Che and coll. with iron-terpyridine complexes[39] and Jensen and coll. with iron scorpionates.[40,44] In both systems Hammett correlations reveal dominant inductive electronic effects (ρ^+ = -0.72 and -0.58, respectively). A similar study by Stavropoulos and coll. using a tripodal trisanilide Fe complex revealed an intermediate behavior with equally important radical delocalization and inductive electronic effects.[43]

We also observed dominant inductive electronic effects ($\rho^+ \approx$ -0.8) when styrene was reacted with phenyltosyliodinane (PhI=NTs) in the presence of phenolate mono- and dinuclear Fe complexes (Scheme S1).[42,46] In this reaction, imido Fe^{IV} species are formed which are active in

NTs transfer.[47,48] A joint experimental and computational study revealed a stepwise mechanism with a significant charge transfer from styrene C_β carbon to imido N in the first transition state involved in the rate determining step. This observation explains why the reaction is dominated by inductive electronic effects with the EA of the active species playing a major role. A very recent study by Jenkins and coll. using tetracarbene macrocycles confirmed this two step mechanism with a rate determining initial step.[45] But Hammett correlations were not reported and the importance of inductive electronic effects was therefore not assessed. Finally, a recent study of olefin aziridination using a Fe^{IV}-nitride catalyst revealed that the reaction is governed by an inverse electronic effect with a nucleophilic active species.[49]

To try and understand these disparate behaviors, we decided to turn our attention to a purely nitrogen-based ligand system and study the mechanism of styrene aziridination by the N^6-ligated iron complex $[(N4Py)Fe^{IV}(NTs)]^{2+}$ species (Scheme 1). $\mathbf{1^{IV}{=}NTs^{2+}}$ has so far been the most thoroughly studied Fe-imido complex.[21,35] Despite the fact that its implication in sulfimidation and $H^\bullet$ abstraction has been characterized in detail,[31,34] its capacity to catalyze styrene aziridination has only been mentioned several years ago.[50] A further interest of this system resides in the easy replacement of two pyridines by other nitrogen donors, e.g. benzimidazole or quinoline, which allows the electronic properties of the complexes to be tuned. The quinoline ligand 2PyN2Q was introduced recently[51] and used to prepare copper, zinc and manganese complexes.[51,52] Very interestingly, its oxo-Fe^{IV} complex $[(2PyN2Q)Fe^{IV}(O)]^{2+}$ species $\mathbf{2^{IV}{=}O^{2+}}$ was described very recently (Scheme 1) and compared to its N4Py counterpart $[(N4Py)Fe^{IV}(O)]^{2+}$ species ($\mathbf{1^{IV}{=}O^{2+}}$).[53–55] Comparison of their reactivities in O transfer to thioanisole[53,55] and HAT from benzylalcohol[55] or cyclohexane[53] revealed a significantly higher activity of $\mathbf{2^{IV}{=}O^{2+}}$ which was attributed to a combination of steric and electronic factors. In this

respect, it is noteworthy that on going from $\mathbf{1^{IV}{=}O^{2+}}$ to $\mathbf{2^{IV}{=}O^{2+}}$ the UV-visible absorption characteristic of Fe^{IV} shifts from 695 to 770 nm. This absorption was assigned to a ligand field transition within the Fe^{IV} d orbital manifold[56] and this bathochromic shift evidences a ca 1400 cm^{-1} lowering of the ligand field on going from $\mathbf{1^{IV}{=}O^{2+}}$ to $\mathbf{2^{IV}{=}O^{2+}}$ in line with the lowered donation of quinoline vs pyridine.

We expected that the lowered donating ability of the 2PyN2Q ligand would increase the EA of the imido complex ($EA_{\mathbf{2NTs}} > EA_{\mathbf{1NTs}}$) and the aziridination efficiency. Therefore we prepared the active species $\mathbf{2^{IV}{=}NTs^{2+}}$ and characterized it by spectroscopic techniques and its electronic structure was assessed by DFT calculations. Comparison of the catalytic activities in styrene aziridination of the systems $\mathbf{1^{II}(NCCH_3)^{2+}}$/PhI=NTs and $\mathbf{2^{II}(NCCH_3)^{2+}}$/PhI=NTs revealed a higher activity of the latter while both show similar major inductive electronic effects. Finally, DFT calculations show again that EA is the main factor ruling the efficacy of the systems and analyses of the reaction profiles confirm that it operates through the transition state of the C-N bond forming rate-determining step. We subsequently extended our computational analysis to the Fe systems published by the groups of Jenkins and Betley,[41,57] which allowed us to show that both systems operate along the similar two-step mechanism with a first step governed by EA. Eventually a general reactivity framework emerges from these combined experimental and computational investigations allowing one to rationalize Fe-catalyzed aziridination.

RESULTS

Synthesis and characterization. The starting complex $\mathbf{[1^{II}(OTf)](OTf)}$ and its tosylimido derivative $\mathbf{1^{IV}{=}NTs^{2+}}$ were prepared according to standard procedures. The starting complex $\mathbf{[2^{II}(OTf)](OTf)}$ was obtained as already described[53,54] and its treatment with 5 eq of PhI=NTs in

acetonitrile at room temperature furnished the tosylimido derivative $\mathbf{2^{IV}=NTs^{2+}}$. This formulation was supported by an ElectroSpray Ionization-Mass Spectra (ESI-MS) analysis of the solution that revealed two peaks at *m/z* 346.0 and 840.9 assigned respectively to the dication $\mathbf{[(2PyN2Q)Fe^{IV}(NTs)]^{2+}}$ (Figure 1) and the monocation $\mathbf{\{[(2PyN2Q)Fe^{IV}(NTs)](OTf)\}^{+}}$ (Figure S1) on their perfect match with the calculated mass spectra. In addition, an intense peak is present at *m/z* 689 corresponding to the monocation $\mathbf{\{[(2PyN2Q)Fe^{III}(OH)](OTf)\}^{+}}$ which may be formed by successive $H^{\bullet}$ abstraction by $\mathbf{2^{IV}=NTs^{2+}}$ and hydrolysis of the resulting $\mathbf{2^{III}\text{-}NHTs^{2+}}$. The formation of $\mathbf{2^{IV}=NTs^{2+}}$ was monitored by UV-visible spectroscopy by the appearance of a NIR absorption at 747 nm (Figure 1c). A similar band appears at 660 nm in $\mathbf{1^{IV}=NTs^{2+}}$ and is characteristic of Fe^{IV} d-d transition.[21,56] Comparison of the energies of the two transitions reveals that the ligand field of the N4Py ligand is stronger by ca 1750 cm^{-1} than that of 2PyN2Q, a value consistent with that found for the oxo analogs (1400 cm^{-1}). In addition to this d-d transition, a more intense absorption at higher energy was reported for $\mathbf{1^{IV}=NTs^{2+}}$ at 445 nm and assigned to a ligand-to-metal charge transfer.[34] This band is present in $\mathbf{2^{IV}=NTs^{2+}}$ also (Figure 1c), together with an additional absorption at slightly lower energy (λ_{max} = 508 nm). It is noteworthy that bands in the same energy range have been reported by the groups of Neidig (472 nm) and Costas (445 nm) for Fe imido complexes of related pentanitrogen ligands. There is no such absorption in this domain in the oxo analogs and it can therefore be viewed as characteristic of the Fe(IV) imido group in these environments. This prompted us to investigate the origin of this transition through TD-DFT calculations (see below).

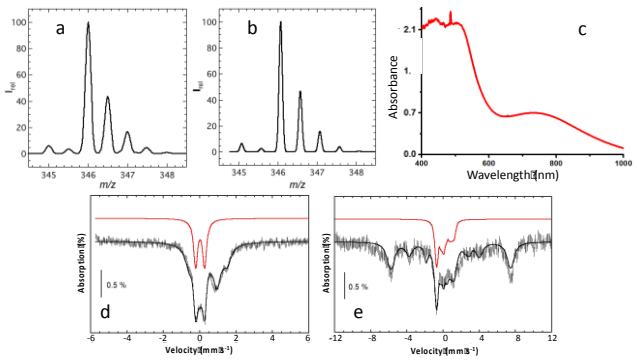

Figure 1. a: ESI-MS of the solution showing the peak at *m/z* 346 associated to **[2^{IV}=NTs]$^{2+}$**; b: calculated spectrum of **[2^{IV}=NTs]$^{2+}$**; c: UV-visible spectrum of **2^{IV}=NTs^{2+}**; d: Mössbauer spectrum of **{[2^{IV}=NTs](OTf)}$^{+}$** recorded at 80 K in absence of magnetic field; e: Mössbauer spectrum of **{[2^{IV}=NTs](OTf)}$^{+}$** recorded at 6 K under a magnetic field of 7 T applied parallel to the γ–ray. Vertical bars experimental data, black line full simulation, red line contribution of Fe^{IV}, see Table S1 for the fit parameters.

The generation of **2^{IV}=NTs^{2+}** was then repeated in acetone using ^{57}Fe-enriched **[2^{II}(OTf)](OTf)** and monitored by UV-visible spectroscopy. When the absorption band at ca 750 nm maximized (after ca 1-2 min) a sample was rapidly frozen and studied by Mössbauer spectroscopy. The spectrum recorded at ca 6 K (Figure 1d) is dominated by a doublet at $\delta \sim 0$ mm s^{-1} flanked on its high energy side by two broad shoulders. Deconvolution of the spectrum revealed the presence of a species (29 %) with an isomer shift ($\delta = 0.02$ mm s^{-1}) and a quadrupole splitting ($\Delta E_Q = 0.54$ mm s^{-1}) consistent with a S = 1 Fe^{IV} species. This spin state was further confirmed by an experiment performed under an applied field of 7 T (Figure 1e). The remaining part of the spectrum was contributed by high-spin Fe^{III} species which originate from the intrinsic decay of the Fe^{IV} species. To validate this assignment, 250 eq thioanisole was added to the frozen Mössbauer cup and it

was thawed above acetone melting point (-95°C) for 3-4 min and frozen again. The new 80 K Mössbauer spectrum (Figure S2b) did not show the original doublet and a new peak at ca 3 mm s^{-1} had appeared, which is consistent with a high-spin Fe^{II} species. This spectrum could indeed be fitted to a mixture of **[2^{II}(OTf)](OTf)** (δ = 1.14 mm s^{-1}, ΔE_Q = 0.54 mm s^{-1}, 43 %) and high-spin Fe^{III} compounds. These observations suggest that **2^{IV}=NTs^{2+}** in the sample reacted with thioanisole to give the sulfylimine Ph-S(NTs)-Me, thereby regenerating the starting Fe^{II}.

Electronic structure of 2^{IV}=NTs^{2+} and comparison to 1^{IV}=NTs^{2+}. Both **2^{IV}=NTs^{2+}** and **1^{IV}=NTs^{2+}** were studied by DFT computation in order to get some insights into their electronic structure. A Fe^{IV} ion gives rise to three integer spin states i.e. S= 0, 1 or 2 so geometry optimizations were first carried out for **2^{IV}=NTs^{2+}** and **1^{IV}=NTs^{2+}** for these three spin multiplicities (Table S2). Their structures are shown in Figure 2. Using the B3LYP functional, the triplet state was found to be the ground state in both cases, in agreement with our and published[21] experimental Mössbauer studies. In both cases, the first excited spin state is the quintet, but it is noteworthy that the triplet-quintet energy gap is smaller for **2^{IV}=NTs^{2+}** (3.2 kcal mol^{-1}) than for **1^{IV}=NTs^{2+}** (8.5 kcal mol^{-1}). These observations hold for various density functional methods tested with different amounts of exact exchange (Table S2).

The Fe-N_{Ts} distances obtained for ^{3}**2^{IV}=NTs^{2+}** and ^{3}**1^{IV}=NTs^{2+}** are in the expected range (ca 1.71-1.73 Å, Table S2) and consistent with values already published[21,31,58,59] for ^{3}**1^{IV}=NTs^{2+}**. In agreement with these previous papers the spin densities reveal a strong radical character on the NTs nitrogen (Table S2), especially for the triplet state, reflecting

the high covalency of Fe-imido bonds[59] as can be seen on the Kohn-Sham orbitals displayed in Figure S3 and S4.

The comparison of the electronic absorption spectra of $\mathbf{1^{IV}{=}NTs^{2+}}$ and $\mathbf{2^{IV}{=}NTs^{2+}}$ shows that both have NIR d-d absorptions in the 600 - 800 nm range and a LMCT transition at 445 nm but that an additional band is present at slightly lower energy (λ_{max} = 508 nm) for $\mathbf{2^{IV}{=}NTs^{2+}}$ (Figure 1c). To better understand these evolutions, we have carried out TD-DFT calculations (see SI for computational details) of both complexes. Drawbacks in this methodology are clearly identified such as shifts in the calculated maxima vs experimental ones, and the presence of spurious charge-transfer states due to incorrect asymptotic behaviour of most of the functionals.[60,61] In spite of these issues that can be partly corrected using hybrid or range-separated functional, our TD-DFT spectra reproduce all the experimental trends (see Fig. S5 and S6), whatever the chosen hybrid functional. Indeed an intense band is present at low wavelength for both complexes (*ca* 300-350 nm depending on the functional). A second intense one appears at higher wavelengths for $\mathbf{2^{IV}{=}NTs^{2+}}$, while in both cases weak bands are present in the 600 to 800 nm region. This is examplified in the superposition of the B3LYP spectra given in Fig. S7. Table S3 gathers the main components of the transitions in terms of d-d, LMCT (ligand-metal charge transfer) and π-π* (ligand to ligand charge transfer) character. For $\mathbf{1^{IV}{=}NTs^{2+}}$, the most intense band appearing in the simulated spectrum between 300-400 is attributed mainly to $N_{Ts} \rightarrow$ d transitions while the ligand $\pi_{(py)}$ to d transitions appear at $\lambda < 310$ nm. Some π–π* transition of ligands are also seen in this region. Experimentally this band is observed at *ca* 440 nm, and interestingly is absent or weaker in the case of the oxo analogue.[21] For $\mathbf{2^{IV}{=}NTs^{2+}}$, these transitions are still present and the main evolution is the presence of another intense band between 400-500 nm in the simulated spectrum and at *ca* 510 nm in the experimental one. From

the analysis shown in Table S4 it can be attributed to transitions involving the quinoline group, either LMCT or π–π* ones. These attributions are consistent with the molecular orbitals diagrams shown on Figures S3 and S4, where we observe that the highest occupied molecular orbitals in $\mathbf{2^{IV}{=}NTs^{2+}}$ are localized on the quinoline group.

The Mössbauer parameters calculated in the triplet ground state for both imido species (Table S5) are also in agreement with experimental values, especially for the quadrupole splitting ($\Delta E_Q^{(calc)}$ = 0.57 mm s^{-1} vs $\Delta E_Q^{(exp)}$ = 0.54 mm s^{-1} for $\mathbf{2^{IV}{=}NTs^{2+}}$). The isomer shift δ is less well reproduced (0.17 versus 0.023) as had been already noticed in the previous study on $\mathbf{1^{IV}{=}NTs^{2+}}$.[21] This is certainly related to the high covalency in Fe-imido bonds as above mentioned.

Two key structural features deserve comparison to the recently published X-ray structure of $\mathbf{2^{IV}{=}O^{2+}}$.[53] First, in $\mathbf{2^{IV}{=}NTs^{2+}}$, some H atoms of the quinoline groups are only at 2.08-2.16 Å from the NTs nitrogen (H_Q in Figure 2), which matches the corresponding H-O distance (2.16 Å) in $\mathbf{2^{IV}{=}O^{2+}}$ determined by X-ray crystallography. The equatorial Fe-N distances from the quinoline ligand are also longer than the ones from the pyridine groups (see Table S2). Furthermore, a tilt of the Fe-NTs bond in $\mathbf{2^{IV}{=}NTs^{2+}}$ is evidenced by the N_{ax} – Fe – N_{Ts} angle being 170° while in $\mathbf{1^{IV}{=}NTs^{2+}}$ this angle has increased to 177°. The same behavior was revealed by the X-ray structures of the oxo homologues[53] with an angle of 170.5° for $\mathbf{2^{IV}{=}O^{2+}}$ and of 179° for $\mathbf{1^{IV}{=}O^{2+}}$. Overall the optimized geometry of $\mathbf{2^{IV}{=}NTs^{2+}}$ reveals a strong similarity to $\mathbf{2^{IV}{=}O^{2+}}$.

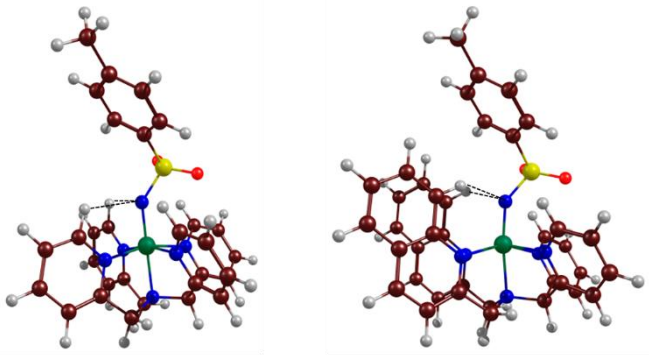

Figure 2. Molecular structures of complexes $\mathbf{1^{IV}}$=$\mathbf{NTs^{2+}}$ (left) and $\mathbf{2^{IV}}$=$\mathbf{NTs^{2+}}$ (right), optimized at B3LYP-D3/BS1 level of theory. N_{Ts}…H interactions are shown as dashed lines.

The evolutions of the equatorial Fe-N distances as well as of the energy difference between the triplet ground state and the quintet first excited state are consistent with the features of the two ligands as already stated by Que et al.[53] A weaker ligand field from 2PyN2Q compared to N4Py could be anticipated due to i) its less basic character and ii) the longer Fe-N distances due to steric effects, and evidenced by the electronic spectra. It explains why the quintet state is lower for $\mathbf{2^{IV}}$=$\mathbf{NTs^{2+}}$ than for $\mathbf{1^{IV}}$=$\mathbf{NTs^{2+}}$. The same behavior in the spin states orderings had been traced in the oxo complexes from their reactivity and the increase in ZFS (zero-field splitting) from the N4Py to the 2PyN2Q Fe^{IV}-oxo complex.[53]

The DFT estimations of electron affinities (Table S6) reveal a higher value for $\mathbf{2^{IV}}$=$\mathbf{NTs^{2+}}$ (139 kcal mol^{-1}) than for $\mathbf{1^{IV}}$=$\mathbf{NTs^{2+}}$ (130.5 kcal mol^{-1}). This *ca* 9 kcal mol^{-1} difference is probably contributed by (i) the less basic and donating character of the 2PyN2Q ligand, and (ii) the stronger N_{Ts}…H interactions in $\mathbf{2^{IV}}$=$\mathbf{NTs^{2+}}$ compared to those in $\mathbf{1^{IV}}$=$\mathbf{NTs^{2+}}$ (Figure 2).

Comparison of the catalytic nitrene transfer activities of 1^{IV}=NTs^{2+} and 2^{IV}=NTs^{2+}. The ability of **[1^{II}(OTf)](OTf)** and **[2^{II}(OTf)](OTf)** to catalyze styrene aziridination was assayed in acetonitrile at room temperature with a catalyst/PhI=NTs/substrate ratio of 0.05/1/10. After 6 h of reaction, the yield of aziridine obtained with **[1^{II}(OTf)](OTf)** was lower than that with **[2^{II}(OTf)](OTf)** (59 vs 70 %). This is in agreement with the higher EA of **2^{IV}=NTs^{2+}** than **1^{IV}=NTs^{2+}** ($EA_{2NTs} > EA_{1NTs}$) and hence its higher reactivity.

Table 1. Distribution of products in competitive styrene aziridination experiments. Y_X and Y_H are the respective yields of *p*-X-substituted styrene and styrene determined by ^{1}H NMR.

Styrene	**1^{IV}=NTs^{2+}**	**2^{IV}=NTs^{2+}**
p-X subst.	Y_X / Y_H	Y_X / Y_H
NO_2	20 / 80	15 / 85
CN	24 / 76	19 / 81
CF_3	25 / 75	22 / 78
Cl	48 / 52	48 / 52
Me	66 / 34	65 / 35
tBu	66 / 34	70 / 30
OMe	67 / 33	83 / 17

Conditions: catalyst / iodinane / styrene / *p*-substituted styrene 0.05 : 1 : 5 : 5. Solvent: acetonitrile, room temperature, 6h

When cis-stilbene was used as substrate under the same conditions the trans-aziridine was formed with both catalysts, in very high amount (87 %) with **[2^{II}(OTf)](OTf)** and almost exclusively (97%) with **[1^{II}(OTf)](OTf)**. These results clearly support a stepwise aziridination mechanism. In order to get a deeper insight into the reactivities of the two catalysts, competition experiments between styrene and a *p*-substituted styrene have been carried out to build Hammett correlations and the results are summarized in Table 1.

The log of the ratios of the respective yields of styrenes in these competition experiments correlate linearly with the σ^+ inductive parameter (Figure 3). Excellent correlations are obtained indeed ($R^2 > 0.99$) for both compounds and the negative slopes indicate that the active species in nitrene transfer is electrophilic. The values of these slopes (N4Py: $\rho^+ = -0.83$; 2PyN2Q: $\rho^+ = -0.94$) are consistent with a higher sensitivity of 2PyN2Q to inductive electronic effects.

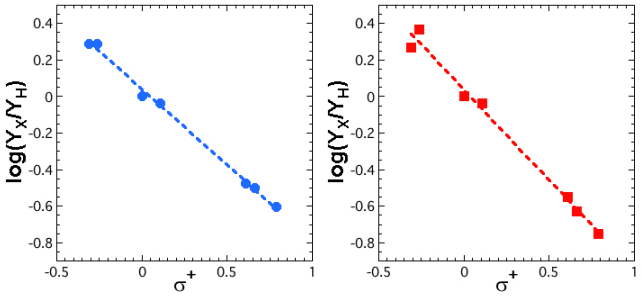

Figure 3. Hammett correlations for styrene aziridination by **[1^{II}(OTf)](OTf)** (left, $\rho^+ = -0.83$, $R^2 = 0.998$) and **[2^{II}(OTf)](OTf)** (right, $\rho^+ = -0.94$, $R^2 = 0.994$).

DFT calculations mechanism: reaction pathways with styrene. The Hammett plots are consistent with a rate determining step involving a charge transfer from styrene to the active species, as found in our previous aziridination studies[42,46] which revealed a two-step mechanism (Scheme 2). We thus investigated reaction profiles of styrene attack onto the Fe^{IV}-imido active species for both complexes along these lines and the computed pathways are shown in Figure 4 (see Tables S7 and S8 for detailed thermodynamics data).

Scheme 2. Stepwise mechanism for aziridination involving a carbon radical intermediate.

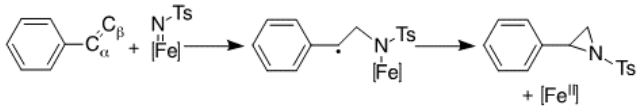

For complex $\mathbf{1^{IV}{=}NTs^{2+}}$, the first TS could be identified on each of the spin surfaces for the attack onto styrene C_β atom (Scheme 2). The activation enthalpy is lower for the quintet state (9.7 kcal mol^{-1}) than for the triplet state (20.9 kcal mol^{-1}) and singlet state (15.6 kcal mol^{-1}). For singlet and quintet states, an electron transfer takes place after the TS so that the forward product is the final aziridine with regeneration of the Fe^{II} complex. In the case of the triplet state, the Fe^{III} – styrenyl radical intermediate is obtained and a second step is necessary to yield the aziridine. The TS for this process could not be identified even after several very tight scans with a constrained reaction coordinate (C-N distance, C-C-N angle) thus the activation barrier was approximated as the electronic energy difference between the scan maximum and the intermediate.

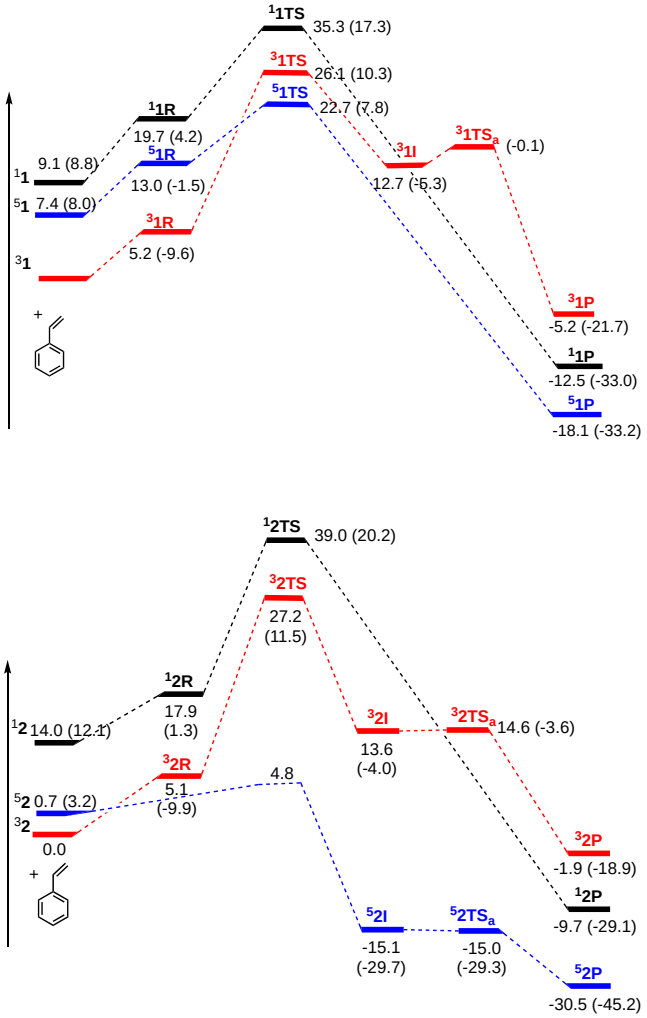

Figure 4. Reaction pathways showing free energies and electronic energies in parentheses (kcal mol^{-1}) for styrene aziridination from B3LYP-D3 BS2COSMO//B3LYP-D3/BS1 computations for **1**^{IV}**=NTs**$^{2+}$ (top) and **2**^{IV}**=NTs**$^{2+}$ (bottom). Black: singlet channel, red: triplet channel, blue : quintet channel. For ^{5}**2**^{IV}**=NTs**$^{2+}$, the blue dotted line visualizes the free energy barrier calculated with Marcus law.

In the case of complex **2**^{IV}**=NTs**$^{2+}$, we observe reaction profiles highly dependent on each spin surface. In particular, the triplet and singlet states show a high free energy activation barrier for the attack of styrene C_β onto $Fe^{IV}NTs$ group after the formation of a preorganized reactant system, being 22.1 kcal mol^{-1} for the triplet and *ca* 21.1 kcal mol^{-1} for the singlet. By contrast, on

the quintet surface no reactant minimum could be characterized, and an electron transfer occurs to yield an intermediate very close to formation of the aziridine with a reduced Fe^{II} species and a cationic styrene group. Indeed, an energy optimization process starting with complex ^{5}**2^{IV}=NTs^{2+}** and styrene at more than 6 Å (styrene C_β - N_{Ts} distance) converges straightforwardly to this intermediate. From the latter, an almost barrierless pathway leads to the expected aziridine and regeneration of the Fe^{II} complex ready for reaction with a subsequent NTs donor. This long distance electron transfer is similar to the behavior observed for **1^{IV}=NTs^{2+}**.[31,34] We have thus calculated the activation energy of this transfer using Marcus law and found a free energy barrier of 4.1 kcal mol^{-1} (see Table S9 and SI for details). This electron transfer is also observed when geometry optimizations are run in a solvent continuum medium. This behavior is thermodynamically consistent with the value of the one-electron oxidation potential of styrene, calculated at the same computational level as EAs, to be 138.7 kcal mol^{-1}, very similar to the EA of complex **2^{IV}=NTs^{2+}**. Therefore although complex **2^{IV}=NTs^{2+}** exhibits a triplet ground state, the quintet surface may provide a much more favorable channel. Such situation is reminiscent of the multistate reactivity first described by Shaik[62–64] in Fe oxo systems**.**

The structure and electronic features (Mulliken group spin densities and charges) of the first TS and of the intermediate - when present - are summarized in Figures S8-S11 for **1^{IV}=NTs^{2+}** and **2^{IV}=NTs^{2+}**. These results are consistent with an electrophilic reactivity of the high-valent Fe active species where the activation barrier is driven by the charge transfer between styrene and the active species. Indeed for the quintet surface of **2^{IV}=NTs^{2+}**, this intermediate is close to the aziridine product as a second electron has been transferred prior to cyclization.

The product in all cases is an iron(II) complex with the aziridine coordinated either by the N atom or by an oxygen from the SO_2 group (Figure S12) with the exception of $^{1}\mathbf{2^{IV}{=}NTs^{2+}}$ (see SI).

Extension of the DFT analysis to other systems.

Jenkins and coll. have reported two generations of tetracarbene macrocycles whose Fe imide complexes catalyze alkenes aziridination from alkyl or aryl azides.[57,65] Their recent DFT analysis[45] of the reaction profile revealed a two-step mechanism, where the initial formation of the C - N bond is rate determining as we found.[42,46] To further analyze their behavior we computed the charges developing in the first transition state TS1 and found that a small charge transfer (ca 0.2 e^-) occurs from decene to the imido nitrogen (Table S10). Consistently, these catalysts have small EAs (Table S6) and they operate in significantly harsher conditions (substrate used as solvent, long time and temperatures in the range 80 - 90 °C) than our standard ones. It follows that EA drives the activity of these systems also.

By contrast to most Fe systems,[39,40,42–44,46] Hammett correlations have shown that inductive effects are negligible for Betley's Fe catalyst[41] whose reactivity is ruled by radical delocalization, suggesting a two-step mechanism. Surprisingly, aziridination of *cis*-β-deuterostyrene produced exclusively *cis*-1-adamantyl-2-deutero-3-phenylaziridine, a feature usually associated to a concerted mechanism. This lack of isomerization was tentatively ascribed to "radical combination out-competing C-C bond rotation". Therefore Betley's system appears to behave in a peculiar manner. In order to get a complete understanding of iron-catalyzed aziridination we investigated it more in depth. At first, we calculated EA of its purported active species formulated as ($^{DCP}L^{Ad}$)FeCl(NAd) $\mathbf{4'^{III}Cl\text{-}^{\bullet}NAd}$: the value obtained (88.9 kcal mol^{-1}) is ca 20 kcal mol^{-1} smaller than that of our least active catalyst. With the same DFT procedure (see SI for

details), we then calculated the reaction profile of styrene aziridination using a model of **4'^{III}Cl-$^{\bullet}$NAd** where adamantyl groups were replaced by *t*Bu ones (Figure S13). A two-step mechanism was found (Figure 5) which is very similar to ours as long as molecular events are concerned: formation of the C-N bond leading to an Fe^{III} and a benzyl radical and subsequent closure of the aziridination ring and release from the catalyst whose iron has been reduced. Instead, a decisive difference was found in the energetics of the reaction: indeed whereas in most cases forming the C-N bond is more energetic than closing the aziridine ring and is thus rate determining,[42,45,66,67] the reverse is found for Betley's catalyst. As a matter of fact, the electronic energy barrier (15.6 kcal mol^{-1}) which was obtained from very tight relaxed scans (Figure S14) for aziridine closure is significantly higher than the activation energy of C-N bond formation (11.5 kcal mol^{-1}).

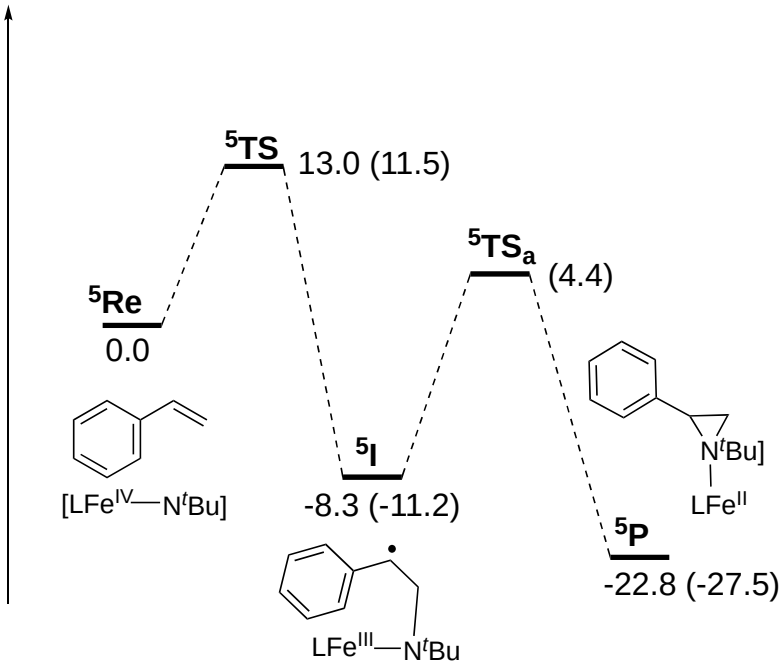

Figure 5. Reaction pathway showing free energies (kcal mol^{-1}) and electronic energies in parentheses for styrene aziridination from B3LYP-D3 BS2COSMO//B3LYP-D3/BS1 computations for the model of **4'^{III}Cl-$^{\bullet}$NAd** (see text)**.**

This finding fully explains the dominance of radical delocalization that, in this case, is due to the difficulty in forming the aziridine ring from the benzyl radical. This difficulty can be traced to two factors: (i) the bulkiness of the ligand substituents hinders the rotation of the substrate necessary to close the aziridine ring and (ii) the structure of the intermediate ^{5}**I** in the reaction profile (Figure S15) reveals a π–π□interaction between styrene aromatic ring and the ligand dipyrrolic group. Both features explain that the observed stereoselectivity in the aziridination of cis-β–deuterostyrene catalyzed by **4'^{III}Cl-$^{\bullet}$NAd**[41] is of steric origin and not associated to a concerted mechanism. As a matter of fact, as highlighted by Perez, Maseras and coll. for Cu and Ag systems,[7] a concerted mechanism leading to retention of configuration is associated to a closed-shell (singlet) configuration of the metal-nitrene unit. Similar closed-shell singlet configuration of Fe-nitrene units are extremely rare because they require a very strong equatorial ligand field. As a matter of fact, only two examples of Fe^{IV}=NR complexes with a tetracarbene macrocycle have been very recently described by Jenkins and coll.. Unfortunately, these complexes were reported to be unable to transfer the nitrene group to olefins even at temperatures as high as 80 °C.[30] In most cases, the closed-shell singlet state of high-valent Fe species is strongly destabilized with respect to the triplet and quintet states by 10 to 25 kcal mol^{-1}.[42,43,68] Consequently, they are unlikely to play a significant role in nitrene transfer. Hence, the observed retention configuration must be caused by steric hindrance to the rotation around the C-C bond in the intermediate, as proposed by Betley and coll.[41] and pinpointed in the present study.

DISCUSSION

In the present work we have compared the aziridination efficacies of the active tosylimidoiron(IV) species derived from the N4Py and 2PyN2Q ligands to validate the dominant role of EA and its predictive value. In the following paragraphs we will address two specific questions: (i) can the EA of the active species explain the reactivity of a wide range of Fe catalysts? and (ii) can it rationalize diverse behaviors observed in literature and explain the peculiarity of the system described by Betley and coll.?[41]

Rationalization of experimental data. Considering the first issue, our results are in complete agreement with the expectations: if the 2PyN2Q ligand were less electron-donating than N4Py, it would lead to an active species with a higher EA. Indeed, DFT calculations confirmed this expectation and quantified the estimated difference to *ca* 9 kcal mol^{-1} (**2^{IV}=NTs^{2+}** 139 kcal mol^{-1} vs **1^{IV}=NTs^{2+}** 130.5 kcal mol^{-1}). Catalytic aziridination experiments revealed a higher activity of 2PyN2Q vs N4Py (70 vs 59 %), perfectly in line with the calculations. This observation is consistent with our previous findings using mono- and dinuclear aminophenolate iron complexes.[69,70] Aiming at evidencing the trend linking aziridination yields (Y) and EA of the active species we have plotted them against each other (Figure 6). It is worth noting that all catalytic aziridination experiments were conducted along the same protocol and that EA of all active species were calculated in the same manner (see Table S13). These data highlight a monotonous and roughly proportional increase in Y from 5 % to 90 % as EA increases from 109 to 143 kcal mol^{-1}. Hammett plots have shown that all catalysts exhibit similar behaviors with ρ^+ values in the range -0.3 to -0.9 in agreement with an electrophilic active species and a partial charge transfer in the rate determining step. Our DFT calculations have shown that all catalysts operate along the same mechanism where the aziridination reaction is initiated by a charge

transfer from styrene C_β to tosylimide. The monotonous character of the observed trend supports that no steric hindrance plays a significant role in the reaction in spite of notable differences in accessibility between the mono iron aminophenolate complexes where the ligands are tetradentate, the pentadentate ligands of this work and the dinuclear complex.[69,70] The absence of steric influence is probably due to the fact that the charge transfer occurring in the rate determining step does not require a close contact of the two reactants.

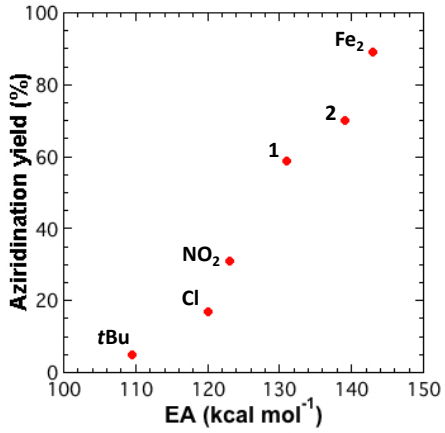

Figure 6. Plot of aziridination yields vs EA of active species. See Scheme S1 for catalysts precursors structures and Table S10 for electron affinities and aziridination yields values.

Electron affinity of the active species. Two factors contribute a high EA of a (ligand)Fe(=NR) active species. The first factor is the nature of R: the more it is electron withdrawing, the higher the EA. Indeed, the observed higher activity of tosylnitrenes vs tolylnitrenes supports this. A DFT calculation allowed us to estimate that EA of (ligand)Fe(NTs) will be ca 20 kcal mol^{-1} higher than that of (ligand)Fe(NTol) (Tol = *p*-tolyl, Table S4). Of course, analogs with an aliphatic nitrene (e.g. *t*Bu, adamantyl) will have an even lower EA. The second factor is the overall charge of the active species which is directly related to the charge of the ligand. For the neutral pentanitrogen ligands

(N4Py and 2PyN2Q) EA ~ 135 kcal mol^{-1}, whereas EA ~ 120 kcal mol^{-1} for the dianionic diphenolate ligands.[42,46] This feature is further illustrated by the study of TAML complexes by Nam and coll.: oxidation of the ligand in $[(TAML)Fe^{V}(NTs)]^{-}$ caused an increase of EA by ca 19 kcal mol^{-1} (from $EA_{\mathbf{3}^{-}}$ = 103.9 kcal mol^{-1} to $EA_{\mathbf{3}^{\bullet}}$ = 122.8 kcal mol^{-1}).[29] For a series of monoiron aminophenolates we found a similar trend between Y and $E(Fe^{III}/Fe^{II})$, the redox potential of the precursor complex, what is consistent with this potential reflecting the ligand electron donation as does EA.[46]

Analysis of Hammett correlations. The importance of EA for thioanisole amination has been rationalized by the comparison of $\mathbf{1{=}O^{2+}}$ vs $\mathbf{1{=}NTs^{2+}}$ which revealed the occurrence of a long range electron transfer for the imido complex.[31] It was further substantiated with the TAML system where the huge increase of EA brought about by TAML oxidation translated into an increase of sulfimidation rate by four orders of magnitude.[29] In the case of aziridination, our previous study has disclosed that the first (rate determining) step of aziridination involves a partial charge transfer from styrene to the nitrene.[42] Owing to the similar oxidation potentials of substituted thioanisoles and styrenes ($E_{1/2}^{ox}$(*p*-X-styrene) - $E_{1/2}^{ox}$(*p*-X-thioanisole) *ca* 0.1 - 0.3 V), the importance of EA for aziridination appears quite logical, albeit it is expected to be smaller than for sulfimidation. Interestingly, this view is supported by the recent work of Jensen and coll.[44] who reported Hammett correlations for thioanisoles sulfimidation and styrenes aziridination by their Fe scorpionate catalysts. Whereas the sulfimidation data gave a good correlation with the σ_p purely inductive parameter with a slope ρ_p = -1.5, the aziridination data gave a poor correlation with this parameter (R^2=0.80). A better correlation (R^2=0.92) was obtained with σ_p^+ which includes resonance effects giving a slope ρ_p^+ = -0.6. Whilst similar correlations are obtained for the two reactions, both the reduced absolute value of the slope and

the necessary inclusion of resonance effects indicate that albeit aziridination is clearly dominated by inductive effects, resonance effects play a minor but noticeable role (see below). Dominant inductive effects were also revealed by Hammett correlations reported for Fe catalysts by Che and coll.[39] and Jensen and coll.,[40,44] Cu catalysts by Müller and coll.[71] and Chang and coll.[72] and for dirhodium tetraacetate by Müller and coll..[71]

CONCLUSIONS

The present data have established the importance of the electron affinity of the species active in NTs transfer for styrene aziridination. Of note is the fact that the higher activity of **2^{IV}=NTs** vs **1^{IV}=NTs** could be predicted from the respective ligand properties. Moreover, this combined experimental and computational study has allowed us to propose a general mechanistic landscape in which the rate-determining molecular event is the formation of the bond between styrene C_β and the Fe-bound imide (nitrene). The corresponding rate-determining transition state involves a charge transfer from styrene to the imide which is governed by the EA of the active species. This scheme most likely holds for all systems exhibiting Hammett correlations revealing significant inductive effects even if they are not dominant. The strong departure from this behavior shown by Betley's system has been traced to steric factors that hinder aziridine ring closure and make the second step rate-determining. Interestingly, intermediate behaviors between these two limiting cases have been reported in the literature for Cu,[7,8] Ag,[7] Ru[73] and some Mn, Co and Fe[43] catalysts. In those systems, inductive and radical delocalization effects are of the same order of magnitude (See Table S12 for a summary of these systems). From the analysis of Betley's catalyst, one may thus envision that an intermediate behavior may result from the similar magnitude of the activation energies of both reaction

steps. Eventually EA emerges as the key parameter and a general descriptor to predict the activity of an Fe catalyst. Literature data and our calculations have concurred to show that the nature of the R substituent on the nitrogen and the overal charge of the active species are the two most important parameters. However one must keep in mind that other processes can intervene at times to blur this picture: (i) formation of the active iron imido species[45,66,67] which may become rate-determining[66,67] and (ii) competitive formations of tetrazene,[45] tetrazoline[67] or imidazoline[42] derivatives.

Notes

The authors declare no competing financial interest.

ACKNOWLEDGMENTS

We thank the reviewers for bringing to our attention the charge transfer band of these imido Fe complexes. We thank Dr J. Pécaut for ESI-MS characterization. J.-M. L. and P. M. thank the Labex ARCANE and CBH-EUR-GS (ANR-17-EURE-0003) for partial funding. The authors thank the COST Network (eCOST BIO) under action CM1305 for support. D. M. acknowledges SERB, India (EMR/2015/000164) for funding to this project. CSIR-India is acknowledged for financial support (fellowship to JP). R. P acknowledges DST, India for INSPIRE Faculty fellowship and SERB, India (CRG/2018/001377) for funding. SR acknowledges SERB-India (SRG/2019/000310). This work was performed using HPC resources from GENCI-CINES (Grant 2016-c2016087 648) and GENCI-IDRIS (Grant 2017-A0020807648).

ASSOCIATED CONTENT

Supporting information

The Supporting Information is available free of charge at https://pubs.acs.org/doi/

Experimental procedures, compound characterization and computational details (PDF)

AUTHOR INFORMATION

Corresponding Authors

Jean-Marc Latour - Univ. Grenoble Alpes, CEA, CNRS, IRIG, LCBM, 38000 Grenoble, France; orcid.org/; Email: jean-marc.latour@cea.fr

Pascale Maldivi - Univ. Grenoble Alpes, CEA, CNRS, IRIG, SYMMES, 38000 Grenoble, France; orcid.org/; Email: pascale.maldivi@cea.fr

Debabrata Maiti- Department of Chemistry, IIT Bombay, Powai, Mumbai-400076, India; orcid.org/; E-mail: dmaiti@chem.iitb.ac.in

Present Addresses

Dr. G. Coin- Department of Chemistry and Applied Biosciences, ETH Zürich, 8093 Zürich, Switzerland

Dr. R. Patra-Amity Institute of Click Chemistry Research & Studies (AICCRS), Amity University, Sector-125, Noida, India

Dr. S. Rana-Department of Chemistry, University of North Bengal, Raja Rammohunpur, Darjeeling, West Bengal-734013, India

Author Contributions

The manuscript was written through contributions of all authors. All authors have given approval to the final version of the manuscript. [&]These authors contributed equally.

REFERENCES

(1) Davies, H. M. L.; Manning, J. R. Catalytic C–H Functionalization by Metal Carbenoid and Nitrenoid Insertion. *Nature* **2008**, *451*, 417–424.

(2) Müller, P.; Fruit, C. Enantioselective Catalytic Aziridinations and Asymmetric Nitrene Insertions into CH Bonds. *Chem. Rev.* **2003**, *103*, 2905–2920.

(3) Roizen, J.; Harvey, M.; DuBois, J. Metal-Catalyzed Nitrogen-Atom Transfer Methods for the Oxidation of Aliphatic C-H Bonds. *Acc. Chem. Res.* **2012**, *45*, 911–922.

(4) Che, C. M.; Yu, W. Y. Ruthenium-Oxo and -Tosylimido Porphyrin Complexes for Epoxidation and Aziridination of Alkenes. *Pure Appl. Chem.* **1999**, *71*, 281–288.

(5) Che, C.-M.; Lo, V. K.-Y.; Zhou, C.-Y.; Huang, J.-S. Selective Functionalisation of Saturated C-H Bonds with Metalloporphyrin Catalysts. *Chem. Soc. Rev.* **2011**, *40*, 1950–1975.

(6) Collet, F.; Lescot, C.; Dauban, P. Catalytic C–H Amination: The Stereoselectivity Issue. *Chem. Soc. Rev.* **2011**, *40*, 1926–1936.

(7) Maestre, L.; Sameera, W. M. C.; Mar Diaz-Requejo, M.; Maseras, F.; Pérez, P. J. A General Mechanism for the Copper- and Silver-Catalyzed Olefin Aziridination Reactions: Concomitant Involvement of the Singlet and Triplet Pathways. *J. Am. Chem. Soc.* **2013**, *135*, 1338–1348.

(8) Bagchi, V.; Paraskevopoulou, P.; Das, P.; Chi, L.; Wang, Q.; Choudhury, A.; Mathieson, J. S.; Cronin, L.; Pardue, D. B.; Cundari, T. R.; Mitrikas, G.; Sanakis, Y.; Stavropoulos, P. A Versatile Tripodal Cu(I) Reagent for C−N Bond Construction via Nitrene-Transfer Chemistry: Catalytic Perspectives and Mechanistic Insights on C−H Aminations/Amidinations and Olefin Aziridinations. *J. Am. Chem. Soc.* **2014**, *136*, 11362–11381.

(9) Olivos Suarez, A. I.; Lyaskovskyy, V.; Reek, J. N. H.; van der Vlugt, J. I.; de Bruin, B. Complexes with Nitrogen-Centered Radical Ligands: Classification, Spectroscopic Features, Reactivity, and Catalytic Applications. *Angew. Chem. Int. Ed.* **2013**, *52*, 12510–12529.

(10) Kuijpers, P. K.; van der Vlugt, J. I.; Schneider, P.; de Bruin, B. Nitrene Radical Intermediates in Catalytic Synthesis. *Chem. Eur. J.* **2017**, *23*, 13819–13829.

(11) Correa, A.; Garcia Mancheno, O.; Bolm, C. Iron-Catalysed Carbon–Heteroatom and Heteroatom–Heteroatom Bond Forming Processes. *Chem. Soc. Rev.* **2008**, *37*, 1108–1117.

(12) Enthaler, S.; Junge, K.; Beller, M. Sustainable Metal Catalysis with Iron: From Rust to a

Rising Star? *Angew. Chem. Int. Ed.* **2008**, *47*, 3317–3321.

(13) Bolm, C. A New Iron Age. *Nat. Chem.* **2009**, *1*, 420–420.

(14) Fürstner, A. Takes To Make This Base Metal a Multitasking Champion. *ACS Cent. Sci.* **2016**, *2*, 778–789.

(15) Lewis, J. C.; Coelho, P. S.; Arnold, F. H. Enzymatic Functionalization of Carbon-Hydrogen Bonds. *Chem. Soc. Rev.* **2011**, *40*, 2003–2021.

(16) Svastits, E. W.; Dawson, J. H.; Breslow, R.; Gellman, S. H. Functionalized Nitrogen Atom Transfer Catalyzed by Cytochrome-P-450. *J. Am. Chem. Soc.* **1985**, *107*, 6427–6428.

(17) Brandenberg, O. F.; Fasan, R.; Arnold, F. H. Exploiting and Engineering Hemoproteins for Abiological Carbene and Nitrene Transfer Reactions. *Curr. Opin. Biotechnol.* **2017**, *47*, 102–111.

(18) Zhang, R. K.; Huang, X.; Arnold, F. H. Selective C-H Bond Functionalization with Engineered Heme Proteins: New Tools to Generate Complexity. *Curr. Opin. Chem. Biol.* **2019**, *49*, 67–75.

(19) Tsutsumi, H.; Katsuyama, Y.; Izumikawa, M.; Takagi, M.; Fujie, M.; Satoh, N.; Shin-ya, K.; Ohnishi, Y. Unprecedented Cyclization Catalyzed by a Cytochrome P450 in Benzastatin Biosynthesis. *J. Am. Chem. Soc.* **2018**, *140*, 6631–6639.

(20) Saouma, C. T.; Peters, J. C. M≡E and M=E Complexes of Iron and Cobalt That Emphasize Three-Fold Symmetry (E≡O, N, NR). *Coord. Chem. Rev.* **2011**, *255*, 920–937.

(21) Klinker, E. J.; Jackson, T. A.; Jensen, M. P.; Stubna, A.; Juhász, G.; Bominaar, E. L.; Münck, E.; Que, L. A Tosylimido Analogue of a Nonheme Oxoiron(IV) Complex. *Angew. Chem. Int. Ed.* **2006**, *45*, 7394–7397.

(22) Bart, S. C.; Lobkovsky, E.; Bill, E.; Chirik, P. J. Synthesis and Hydrogenation of Bis(Imino)Pyridine Iron Imides. *J. Am. Chem. Soc.* **2006**, *128*, 5302–5303.

(23) Holland, P. L. Electronic Structure and Reactivity of Three-Coordinate Iron Complexes. *Acc. Chem. Res.* **2008**, *41*, 905–914.

(24) Nieto, I.; Ding, F.; Bontchev, R. P.; Wang, H.; Smith, J. M. Thermodynamics of Hydrogen Atom Transfer to a High-Valent Iron Imido Complex. *J. Am. Chem. Soc.* **2008**, *130*, 2716–2717.

(25) King, E. R.; Hennessy, E. T.; Betley, T. A. Catalytic C-H Bond Amination from High-Spin Iron Imido Complexes. *J. Am. Chem. Soc.* **2011**, *133*, 4917–4923.

(26) Searles, K.; Fortier, S.; Khusniyarov, M. M.; Carroll, P. J.; Sutter, J.; Meyer, K.; Mindiola, D. J.; Caulton, K. G. A Cis-Divacant Octahedral and Mononuclear Iron(IV) Imide. *Angew. Chem. Int. Ed.* **2014**, *53*, 14139–14143.

(27) Spasyuk, D. M.; Carpenter, S. H.; Kefalidis, C. E.; Piers, W. E.; Neidig, M. L.; Maron, L. Facile Hydrogen Atom Transfer to Iron(Iii) Imido Radical Complexes Supported by a Dianionic

Pentadentate Ligand. *Chem. Sci.* **2016**, *7*, 5939–5944.

(28) Hong, S.; Sutherlin, K. D.; Vardhaman, A. K.; Jan, J. J.; Park, S.; Lee, Y.-M.; Jang, S.; Lu, X.; Ohta, T.; Ogura, T.; Solomon, E. I.; Nam, W. A Mononuclear Nonheme Iron(V)-Imido Complex. *J. Am. Chem. Soc.* **2017**, *139*, 8800–8803.

(29) Hong, S.; Lu, X.; Lee, Y.-M.; Seo, M. S.; Ohta, T.; Ogura, T.; Clémancey, M.; Maldivi, P.; Latour, J.-M.; Sarangi, R.; Nam, W. Achieving One-Electron Oxidation of a Mononuclear Nonheme Iron(V)-Imido Complex. *J. Am. Chem. Soc.* **2017**, *139*, 14372–14375.

(30) Anneser, M. R.; Elpitiya, G. R.; Townsend, J.; Johnson, E. J.; Powers, X. B.; DeJesus, J. F.; Vogiatzis, K. D.; Jenkins, D. M. Unprecedented Five-Coordinate Iron(IV) Imides Generate Divergent Spin States Based on the Imide R-Groups. *Angew. Chem. Int. Ed. Engl.* **2019**, *58*, 8115–8118.

(31) Kumar, S.; Faponle, A. S.; Barman, P.; Vardhaman, A. K.; Sastri, C. V.; Kumar, D.; de Visser, S. P. Long-Range Electron Transfer Triggers Mechanistic Differences between Iron(IV)-Oxo and Iron(IV)-Imido Oxidants. *J. Am. Chem. Soc.* **2014**, *136*, 17102–17115.

(32) Cowley, R. E.; Eckert, N. A.; Vaddadi, S.; Figg, T. M.; Cundari, T. R.; Holland, P. L. Selectivity and Mechanism of Hydrogen Atom Transfer by an Isolable Imidoiron(III) Complex. *J. Am. Chem. Soc.* **2011**, *133*, 9796–9811.

(33) Wilding, M. J. T.; Iovan, D. A.; Wrobel, A. T.; Lukens, J. T.; MacMillan, S. N.; Lancaster, K. M.; Betley, T. A. Direct Comparison of C-H Bond Amination Efficacy through Manipulation of Nitrogen-Valence Centered Redox: Imido versus Iminyl. *J. Am. Chem. Soc.* **2017**, *139*, 14757–14766.

(34) Vardhaman, A. K.; Barman, P.; Kumar, S.; Sastri, C. V.; Kumar, D.; de Visser, S. P. Comparison of the Reactivity of Nonheme Iron(IV)-Oxo versus Iron(IV)-Imido Complexes: Which Is the Better Oxidant? *Angew. Chem. Int. Ed.* **2013**, *52*, 12288–12292.

(35) Vardhaman, A. K.; Lee, Y.-M.; Jung, J.; Ohkubo, K.; Nam, W.; Fukuzumi, S. Enhanced Electron Transfer Reactivity of a Nonheme Iron(IV)–Imido Complex as Compared to the Iron(IV)-Oxo Analogue. *Angew. Chem. Int. Ed.* **2016**, *55*, 3709–3713.

(36) Damiano, C.; Intrieri, D.; Gallo, E. Aziridination of Alkenes Promoted by Iron or Ruthenium Complexes. *Inorganica Chim. Acta* **2018**, *470* (SI), 51–67.

(37) Fingerhut, A.; Serdyuk, O. V.; Tsogoeva, S. B. Non-Heme Iron Catalysts for Epoxidation and Aziridination Reactions of Challenging Terminal Alkenes: Towards Sustainability. *Green Chem.* **2015**, *17*, 2042–2058.

(38) Shehata, M. F.; Ayer, S. K.; Roizen, J. L. Iron(MCP) Complexes Catalyze Aziridination with Olefins As Limiting Reagents. *J. Org. Chem.* **2018**, *83*, 5072–5081.

(39) Liu, P.; Wong, E. L.-M.; Yuen, A. W.-H.; Che, C.-M. Highly Efficient Alkene Epoxidation and Aziridination Catalyzed by Iron(II) Salt + 4,4′,4″-Trichloro-2,2′:6′,2″-Terpyridine/4,4″-Dichloro-4′-O-PEG-OCH3-2,2′:6′,2″-Terpyridine. *Org. Lett.* **2008**, *10*, 3275–3278.

(40) Liang, S.; Jensen, M. P. Half-Sandwich Scorpionates as Nitrene Transfer Catalysts. *Organometallics* **2012**, *31*, 8055–8058.

(41) Hennessy, E. T.; Liu, R. Y.; Iovan, D. A.; Duncan, R. A.; Betley, T. A. Iron-Mediated Intermolecular N-Group Transfer Chemistry with Olefinic Substrates. *Chem. Sci.* **2014**, *5*, 1526–1532.

(42) Patra, R.; Coin, G.; Castro, L.; Dubourdeaux, P.; Clémancey, M.; Pécaut, J.; Lebrun, C.; Maldivi, P.; Latour, J.-M. Rational Design of Fe Catalyts for Olefin Aziridination through DFT-Based Mechanistic Analysis. *Catal. Sci. Technol.* **2017**, *7*, 4388–4400.

(43) Bagchi, V.; Kalra, A.; Das, P.; Paraskevopoulou, P.; Gorla, S.; Ai, L.; Wang, Q.; Mohapatra, S.; Choudhury, A.; Sun, Z.; Cundari, T. R.; Stavropoulos, P. Comparative Nitrene-Transfer Chemistry to Olefinic Substrates Mediated by a Library of Anionic Mn(II) Triphenylamido-Amine Reagents and M(II) Congeners (M = Fe, Co, Ni) Favoring Aromatic over Aliphatic Alkenes. *ACS Catal.* **2018**, *8*, 9183–9206.

(44) Anderson, C. M.; Aboelenen, A. M.; Jensen, M. P. Competitive Intramolecular Amination as a Clock for Iron-Catalyzed Nitrene Transfer. *Inorg. Chem.* **2019**, *58*, 1107–1119.

(45) Isbill, S. B.; Chandrachud, P. P.; Kern, J. L.; Jenkins, D. M.; Roy, S. Elucidation of the Reaction Mechanism of C2 + N1 Aziridination from Tetracarbene Iron Catalysts. *ACS Catal.* **2019**, *9*, 6223–6233.

(46) Coin, G.; Patra, R.; Clémancey, M.; Dubourdeaux, P.; Pécaut, J.; Lebrun, C.; Castro, L.; Maldivi, P.; Chardon-Noblat, S.; Latour, J.-M. Fe-Based Complexes as Styrene Aziridination Catalysts: Ligand Substitution Tunes Catalyst Activity. *ChemCatChem* **2019**, *11*, 5296–5299.

(47) Avenier, F.; Latour, J.-M. Catalytic Aziridination of Olefins and Thioether Amidation by a Non-Heme Iron Complex. *Chem. Commun.* **2004**, 1544–1545.

(48) Avenier, F.; Gouré, E.; Dubourdeaux, P.; Sénèque, O.; Oddou, J.-L.; Pécaut, J.; Chardon-Noblat, S.; Deronzier, A.; Latour, J.-M. Multiple Aromatic Amination Mediated by a Diiron Complex. *Angew. Chem. Int. Ed.* **2008**, *47*, 715–717.

(49) Crandell, D. W.; Munoz, S. B., III; Smith, J. M.; Baik, M.-H. Mechanistic Study of Styrene Aziridination by Iron(Iv) Nitrides. *Chem. Sci.* **2018**, *9*, 8542–8552.

(50) Klotz, K. L.; Slominski, L. M.; Hull, A. V.; Gottsacker, V. M.; Mas-Balleste, R.; Que, L.; Halfen, J. A. Non-Heme Iron(II) Complexes Are Efficient Olefin Aziridination Catalysts. *Chem. Commun.* **2007**, 2063–2065.

(51) Lo, W. K. C.; McAdam, C. J.; Blackman, A. G.; Crowley, J. D.; McMorran, D. A. The Pentadentate Ligands 2PyN2Q and N4Py, and Their Cu(II) and Zn(II) Complexes: A Synthetic, Spectroscopic and Crystallographic Structural Study. *Inorganica Chim. Acta* **2015**, *426*, 183–194.

(52) Massie, A. A.; Denler, M. C.; Cardoso, L. T.; Walker, A. N.; Hossain, M. K.; Day, V. W.; Nordlander, E.; Jackson, T. A. Equatorial Ligand Perturbations Influence the Reactivity of Manganese(IV)-Oxo Complexes. *Angew. Chem.-Int. Ed.* **2017**, *56*, 4178–4182.

(53) Rasheed, W.; Draksharapu, A.; Banerjee, S.; Young, Jr., V. G.; Fan, R.; Guo, Y.; Ozerov, M.; Nehrkorn, J.; Krzystek, J.; Telser, J.; Que Jr., L. Crystallographic Evidence for a Sterically Induced Ferryl Tilt in a Non-Heme Oxoiron(IV) Complex That Makes It a Better Oxidant. *Angew. Chem. Int. Ed.* **2018**, *57*, 9387–9391.

(54) Rana, S.; Biswas, J. P.; Sen, A.; Clémancey, M.; Blondin, G.; Latour, J.-M.; Rajaraman, G.; Maiti, D. Selective C-H Halogenation over Hydroxylation by Non-Heme Iron(IV)-Oxo: Functional Mimic of Non-Heme Halogenases. *Chem. Sci.* **2018**, *9*, 7843–7858.

(55) Mukherjee, G.; Lee, C. W. Z.; Nag, S. S.; Alili, A.; Reinhard, F. G. C.; Kumar, D.; Sastri, C. V.; de Visser, S. P. Dramatic Rate-Enhancement of Oxygen Atom Transfer by an Iron(Iv)-Oxo Species by Equatorial Ligand Field Perturbations. *Dalton Trans.* **2018**, *47*, 14945–14957.

(56) Decker, A.; Rohde, J.-U.; Klinker, E. J.; Wong, S. D.; Que, L., Jr.; Solomon, E. I. Spectroscopic and Quantum Chemical Studies on Low-Spin Fe-IV=O Complexes: Fe-O Bonding and Its Contributions to Reactivity. *J. Am. Chem. Soc.* **2007**, *129*, 15983–15996.

(57) Chandrachud, P. P.; Bass, H. M.; Jenkins, D. M. Synthesis of Fully Aliphatic Aziridines with a Macrocyclic Tetracarbene Iron Catalyst. *Organometallics* **2016**, *35*, 1652–1657.

(58) Jaccob, M.; Rajaraman, G. A Computational Examination on the Structure, Spin-State Energetics and Spectroscopic Parameters of High-Valent Fe-IV=NTs Species. *Dalton Trans.* **2012**, *41*, 10430–10439.

(59) Sabenya, G.; Gamba, I.; Gomez, L.; Clemancey, M.; Frisch, J. R.; Klinker, E. J.; Blondin, G.; Torelli, S.; Que, L., Jr.; Martin-Diaconescu, V.; Latour, J.-M.; Lloret-Fillol, J.; Costas, M. Octahedral Iron(Iv)-Tosylimido Complexes Exhibiting Single Electron-Oxidation Reactivity. *Chem. Sci.* **2019**, *10*, 9513–9529.

(60) Dreuw, A.; Head-Gordon, M. Failure of Time-Dependent Density Functional Theory for Long-Range Charge-Transfer Excited States: The Zincbacteriochlorin−Bacteriochlorin and Bacteriochlorophyll−Spheroidene Complexes. *J. Am. Chem. Soc.* **2004**, *126* (12), 4007–4016.

(61) Adamo, C.; Jacquemin, D. The Calculations of Excited-State Properties with Time-Dependent Density Functional Theory. *Chem Soc Rev* **2013**, *42* (3), 845–856.

(62) Shaik, S.; de Visser, S.; Ogliaro, F.; Schwarz, H.; Schroder, D. Two-State Reactivity Mechanisms of Hydroxylation and Epoxidation by Cytochrome P-450 Revealed by Theory. *Curr. Opin. Chem. Biol.* **2002**, *6*, 556–567. https://doi.org/10.1016/S1367-5931(02)00363-0.

(63) Shaik, S.; Hirao, H.; Kumar, D. Reactivity of High-Valent Iron–Oxo Species in Enzymes and Synthetic Reagents: A Tale of Many States. *Acc. Chem. Res.* **2007**, *40*, 532–542.

(64) Ye, S. F.; Geng, C. Y.; Shaik, S.; Neese, F. Electronic Structure Analysis of Multistate Reactivity in Transition Metal Catalyzed Reactions: The Case of C-H Bond Activation by Non-Heme Iron(IV)-Oxo Cores. *Phys. Chem. Chem. Phys.* **2013**, *15*, 8017–8030.

(65) Cramer, S. A.; Jenkins, D. M. Synthesis of Aziridines from Alkenes and Aryl Azides with a Reusable Macrocyclic Tetracarbene Iron Catalyst. *J. Am. Chem. Soc.* **2011**, *133*, 19342–19345.

(66) Hopmann, K. H.; Ghosh, A. Mechanism of Cobalt-Porphyrin_Catalyzed Aziridination Kathrin H. Hopmann and Abhik Ghosh. *ACS Catal.* **2011**, *1*, 597–600.

(67) Zardi, P.; Pozzoli, A.; Ferretti, F.; Manca, G.; Mealli, C.; Gallo, E. A Mechanistic Investigation of the Ruthenium Porphyrin Catalysed Aziridination of Olefins by Aryl Azides. *Dalton Trans.* **2015**, *44*, 10479–10489.

(68) Patra, R.; Maldivi, P. DFT Analysis of the Electronic Structure of Fe(IV) Species Active in Nitrene Transfer Catalysis: Influence of the Coordination Sphere. *J. Mol. Model.* **2016**, *22*, 278.

(69) Gouré, E.; Avenier, F.; Dubourdeaux, P.; Sénèque, O.; Albrieux, F.; Lebrun, C.; Clémancey, M.; Maldivi, P.; Latour, J.-M. A Diiron(III,IV) Imido Species Active in Nitrene Transfer Reactions. *Angew. Chem. Int. Ed.* **2014**, *53*, 1580–1584.

(70) Gouré, E.; Senthilnathan, D.; Coin, G.; Albrieux, F.; Avenier, F.; Dubourdeaux, P.; Lebrun, C.; Maldivi, P.; Latour, J.-M. Redox Self-Adaptation of a Nitrene Transfer Catalyst to the Substrate Needs. *Angew. Chem. Int. Ed.* **2017**, *56*, 4305–4309.

(71) Müller, P.; Baud, C.; Jacquier, Y. The Rhodium(II)-Catalyzed Aziridination of Olefins with {[(4-Nitrophenyl)Sulfonyl]Imino}phenyl-L3-Iodane. *Can. J. Chem.* **1998**, *76*, 738–750.

(72) Han, H.; Park, S. B.; Kim, S. K.; Chang, S. Copper-Nitrenoid Formation and Transfer in Catalytic Olefin Aziridination Utilizing Chelating 2-Pyridylsulfonyl Moieties. *J. Org. Chem.* **2008**, *73*, 2862–2870.

(73) Au, S. M.; Huang, J. S.; Yu, W. Y.; Fung, W. H.; Che, C. M. Aziridination of Alkenes and Amidation of Alkanes by Bis(Tosylimido)Ruthenium(VI) Porphyrins. A Mechanistic Study. *J. Am. Chem. Soc.* **1999**, *121*, 9120–9132.